A Heuristic Approach to Reduce Atmospheric Effects in InSAR Data for the Derivation of Digital Terrain Models or for the Characterization of Forest Vertical Structure

Wenjian Ni, Guoqing Sun, Zhiyu Zhang, Yating He, and Zhifeng Guo

***Abstract*—The differences of two digital terrain models (DTMs) derived from airborne interferometric synthetic aperture radar (InSAR) data of short and long wavelengths are utilized for the estimation of vertical forest structures. However, when the spaceborne repeat-pass InSAR data are used, atmospheric effects must be considered. A simple method for the reduction of atmospheric effects in spaceborne repeat-pass interferometry is proposed in this letter. By subtracting a simulated interferogram using the Shuttle Radar Topography Mission (SRTM) DTM from the interferogram of a pair of Phased Array Type L-Band Synthetic Aperture Radar (PALSAR) InSAR data, the remaining phase includes the phase caused by the height differences of scattering phase centers (SPC) at C- and L-bands and the phases caused by atmospheric effects and other changes during the PALSAR repeat-pass period. A low-pass spatial filtering can reveal the atmospheric effect in the phase image because of the low spatial frequency of the atmospheric effects. The proper size of the filtering window can be determined by the changes of standard deviation of filtered phase images as the window size increases. The changes of the standard deviations of the filtered phase images should be almost constant when only the atmospheric effect remains. After reducing the atmospheric effects, the difference between the SRTM-DTM and the PALSAR-DTM was reduced from 60.17 m ± 16.2 m to near 0 m (0.52 m ± 4.3 m) at bare surfaces, and the correlation (R^2) between the mean forest height and the difference between the SRTM-DTM and the PALSAR-DTM was significantly increased from 0.021 to 0.608.**

***Index Terms*—Atmospheric effect, forest height, interferometric synthetic aperture radar (InSAR), interferometry, synthetic aperture radar (SAR).**

I. Introduction

In FORESTED areas, the digital terrain model (DTM) derived from interferometric SAR (InSAR) data is the elevation of the scattering phase center (SPC) rather than that of the ground surface. The SPC is located at a point between the top of the forest canopy and the ground surface; its position is related to the vertical structure of forest canopy as well as to the SAR wavelength. Because a longer wavelength microwave can penetrate deeper into the forest, the height of the scattering phase center (HSPC) of a longer wavelength should be lower than that of a shorter wavelength microwave [1]–[2]. The difference between the two DTMs derived from short- and long-wavelengths data (the penetration difference) can be used to estimate forest height. Kellndorfer *et al.* [3] estimated vegetation height using the difference of the Shuttle Radar Topography Mission (SRTM) data and the National Elevation Datasets (NED) taken as ground surface elevation. The estimation had measurements of $R^2 = 0.79$ (RMSE = 1.1 m) in Georgia and $R^2 = 0.75$ (RMSE = 4.5 m) in California. Neeff *et al.* [1] used the difference between the DTMs from the X- and P-bands as a measure of vegetation height in the estimation of forest biomass. Balzter *et al.* [4] used the X- and L-bands InSAR data acquired by E-SAR airborne sensors to estimate the top heights of forest stands. Praks *et al.* [5] presented results from the FinSAR project, where the E-SAR (operating at the L- and X-bands) and the Helsinki University of Technology Scatterometer (HUTSCAT, operating at the X- and C-bands) instruments were operated together to validate tree-height retrieval algorithms for boreal forest. These studies were based on either single-pass (two antennae, e.g., SRTM) interferometry or airborne SAR data. The InSAR pair was acquired either simultaneously or within a short-time interval. In these instances, it is reasonable to assume that the ground and atmospheric conditions remained the same. However, this assumption was not valid for spaceborne repeat-pass interferometry. For example, the atmospheric condition could not be assumed to be the same for 46-day repeat-pass InSAR data from Phased Array Type L-Band Synthetic Aperture Radar (PALSAR); therefore, atmospheric effects cannot be ignored in spaceborne repeat-pass interferometry.

In measuring terrain deformation or subsidence using differential interferometric SAR (DInSAR), the atmospheric effect in InSAR data has been investigated. Massonnet and Feigl [6] proposed a pair-wise logic method to identify atmospheric effects. It required at least three radar images that were sufficient to form at least two interferometric pairs spanning different intervals. Bock and Williams [7] integrated the measurement of global positioning system (GPS) into the construction of the DTM using InSAR data. Atmospheric delay can be

Manuscript received May 3, 2012; revised July 16, 2012 and February 21, 2013; accepted March 12, 2013. Date of publication May 23, 2013; date of current version November 8, 2013. This work was supported in part by the China MOST 863 Program under grant 2012AA12A306, the National Natural Science Foundation of China under Grants 41001208, 40971203, 41171283, and 91125003, and by the Strategic Priority Research Program-Climate Change: Carbon Budget and Related Issues of the Chinese Academy of Sciences under Grant XDA05050100. Support for the study was also provided by the NASA Terrestrial Ecology Program under Grant NNX09AG66G. The PALSAR data were provided by the Japan Aerospace Exploration Agency (JAXA). The forest inventory map was provided by Lushuihe Forest Bureau of Changbai Mountains.

W. Ni, Z. Zhang, and Z. Guo are with the State Key Laboratory of Remote Sensing Science, Jointly Sponsored by the Institute of Remote Sensing Applications of Chinese Academy of Sciences and Beijing Normal University, Beijing 100101, China (Z. Zhang, e-mail: zhangzy@irsa.ac.cn).

G. Sun is with the University of Maryland, College Park, MD 20742 USA.

Y. He is with the Institute of Geographic Sciences and Natural Resources Research, Chinese Academy of Sciences, Beijing 100101, China.

Color versions of one or more of the figures in this paper are available online at http://ieeexplore.ieee.org.

Digital Object Identifier 10.1109/LGRS.2013.2255579

reduced in the InSAR data using total zenith delay that is estimated from continuous GPS networks [8]. Ferretti *et al.* [9] used the permanent scatterers (PS) identified from a long temporal series of InSAR images to estimate atmospheric phase contributions in InSAR data. These studies provide some solutions for the removal of atmospheric effects under certain conditions with specific requirements. These methods were based on multitemporal InSAR data or required other source data acquired simultaneously with the InSAR data; however, these methods are not practical on a regional scale because of the inaccessibility of auxiliary data. In this paper, we propose a heuristic method to reduce the atmospheric effects in repeat-pass spaceborne InSAR data for the reconstruction of a DTM or for the estimation of mean forest height using a combination of short- and long-wavelengths InSAR data.

II. Methods

Phase differences between short- and long-wavelengths InSAR data were used to estimate the vertical structure of forests in a manner similar to the usage of differential InSAR technology in surface deformation studies in which multiple InSAR data at the same wavelength are utilized. The InSAR interferogram data, such as the repeat-pass PALSAR L-band InSAR data, is mainly determined by the following factors: 1) the changes in atmospheric conditions occurring between the acquisition of master and slave SAR images; 2) the terrain deformation occurring between the acquisition of master and slave SAR images; and 3) the elevation that may be considered as the sum of a digital elevation model (DEM) and the phase center height of objects above the DEM. A bare-ground surface DEM, or a DTM from other InSAR data that does not contain atmospheric effects or surface deformation (e.g., SRTM), may be used to simulate an interferogram. After subtracting the simulated interferogram, the resulting DInSAR phase contains the phase related to the height difference between the PALSAR L-band InSAR phase center and the SRTM DTM; in addition, the DInSAR phase contains the phase components caused by factors 1) and 2) discussed above.

The sensitivities of this DInSAR phase to these factors are different. For the atmospheric effect and terrain deformation that occurred during data acquisition, the change of the propagation delay and path-length is directly related to the phase change as the following [10]:

$$\delta_\phi = 4\pi \frac{\delta_l}{\lambda} \tag{1}$$

Where λ is the wavelength, δ_l is the propagation delay caused by the atmospheric effects or the displacement caused by terrain deformation, and δ_ϕ represents the corresponding phase changes. For the elevation differences between those from two InSAR data δ_h, the corresponding phase is [11]

$$\delta_\phi = 4\pi \frac{\delta_h B}{\lambda \rho \tan\theta} \tag{2}$$

where ρ is the slant range (i.e., the distance from the antenna to ground points), θ is the incidence angle, and B is the baseline length. It may be observed from (1) and (2) that variations in the atmosphere may cause significant errors in elevation difference. For example, if $B = 400$ m, $\lambda = 0.235$ m, $\theta = 34°$, and $\rho = 800$ km, an elevation difference of 39.625 m between two InSAR DTMs causes a phase change of $\pi/2$, the same phase change that would be caused by a change of one-quarter wavelength (0.05875 m) in atmospheric delay or terrain deformation. In other words, if the atmospheric change or terrain deformation of 0.05875 m is not removed, it will cause an error of 39.625 m in the InSAR DTM. The height of most trees is lower than 40 m. If the atmospheric effect or terrain deformation is not minimized, it is impossible to estimate mean forest height by using the penetration difference of two short- and long-wavelengths InSAR DTMs.

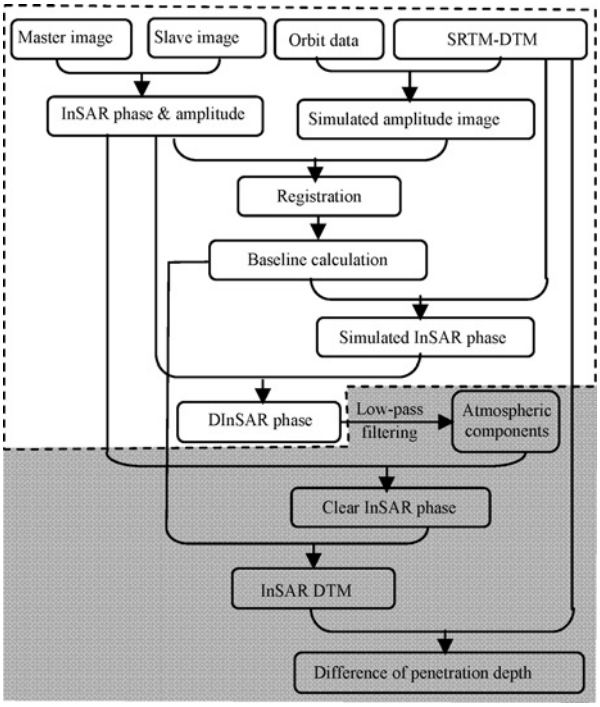

Fig. 1. Workflow of the proposed method.

The sensitivities of the DInSAR phase to terrain deformation and atmospheric effect are the same. These two components are mixed together in the DInSAR phase data. For the measurement of terrain deformation from DInSAR phase data, the atmospheric effects must be accurately removed using the measurement of atmospheric conditions from a GPS signal or another source. To reconstruct the DTM from InSAR data or to estimate the mean forest height from the difference between InSAR DTM and other-sourced DTM/DEM, it is reasonable to assume that no terrain deformation occurs if the repeat cycle of the InSAR data is short (e.g., several tens of days). Therefore, the only phase components in the DInSAR phase image are those related to ground objects and atmospheric effects. Fortunately, the phase components of atmospheric effects should present a spatially low-frequency pattern [11] as opposed to the components of ground objects that are high frequency. Therefore, the atmospheric effect is highlighted as a low-frequency feature in the DInSAR image and can be further extracted by applying a low-pass spatial filter to the DInSAR image.

The SRTM-DTM should be free from atmospheric effects because it was derived from single-pass InSAR data; in this study, it will serve as the other-source DTM/DEM. Fig. 1 shows the workflow of the proposed method. From master and slave single-look complex images, the unwrapped InSAR phase and amplitude images can be obtained following the processes of co-registration, re-sampling, and unwrapping.

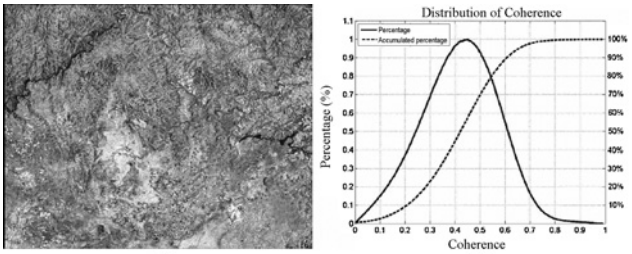

Fig. 2. Coherence image (a) and the probability distribution of coherence (b) of the study area.

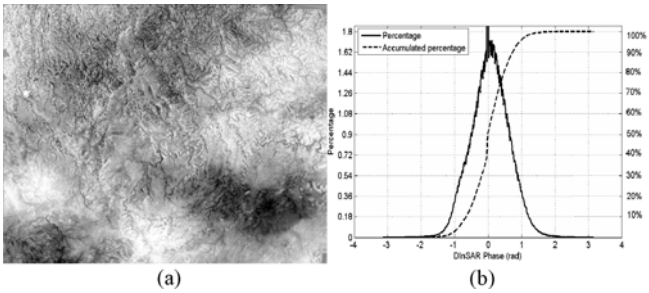

Fig. 3. DInSAR phase image (a) and the probability distribution of the phase (b).

With the orbit data, an SAR amplitude image may be simulated using the SRTM-DTM. The registration is made between the simulated SAR amplitude image and the InSAR amplitude image. The SRTM-DTM is projected into the slant range coordinates using the transformation coefficients from the registration. The baseline may be calculated using the control points selected from the projected SRTM-DTM. With baseline parameters, the InSAR phase image can be simulated using the SRTM-DTM. Subtracting the simulated InSAR phase from the PALSAR InSAR phase may result in the DInSAR phase. The processing steps outlined by the dashed lines in Fig. 1 have been coded in the Repeat Orbit Interferometry Package (ROI_PAC) developed at NASA JPL. The gray shaded area shown in Fig. 1 is the central section of the proposed method. The phase component of atmospheric effects can be retrieved by applying a low-pass spatial filter to the DInSAR phase image. The revealed atmospheric phase is then subtracted from the InSAR phase. An accurate InSAR DTM may be built using the baseline parameters and the corrected InSAR phase. The height difference between the SRTM-DTM and the PALSAR InSAR DTM should be the penetration difference between C- and L-bands.

An essential step in low-pass filtering is determining the window size. If the window size is small, most high-frequency details will remain in the filtered results. As the window size increases, the high frequency details in the filtered image decrease. When the window size is large enough, the filtered image contains only the low-frequency atmospheric effects. The changes in the standard deviation of the filtered image will become steadier with increasing window size, which may then be used as the criterion to determine the window size.

III. Experiments

A. Test Site and Data

The test site (42.5°N, 127.8°E) is a forest in China managed by Lushuihe Forest Bureau near the Changbai Mountains in Fusong County, Jilin Province. The northern part of the area is mountainous, and the central and southern parts are relatively flat; most areas are covered by forest. The InSAR data used in this study was acquired by the PALSAR (HH polarization) on 07/14/2007 and 08/29/2007, respectively.

The basic unit of forest inventory map provided by the Lushuihe Forest Bureau is sub-compartment. The mean forest height of each sub-compartment is given. However, the area of a sub-compartment is several tens of hectares with significant spatial heterogeneity; therefore, it is not feasible to conduct pixel-by-pixel quantitative comparisons with the penetration difference. The forest inventory data were used to show the spatial pattern of forest stands.

Field measurements of the forest were conducted in June 2007. Within the coverage of the PALSAR InSAR data, 18 circle sampling plots with 35 m in radius were established. The diameter at breast height (DBH)—1.3 m above ground—and the height of each tree were measured; the species of tree, its height and its DBH (>5 cm) were recorded. The mean forest heights of these 18 sampling plots were used to quantitatively evaluate the correlation between mean forest height and the penetration difference between the C- and L-bands.

The SRTM data were acquired in February 2000. The SRTM data are distributed in two levels, SRTM-1 for U.S. territory and SRTM-3 for non-U.S. territory. Only SRTM-3 data are available at the test site.

B. Results

Fig. 2 shows the spatial and probability distribution of the InSAR coherence. The peak of the coherence is approximately 0.45, while the coherence of almost 70% of the pixels is larger than 0.35. Fig. 3 shows the DInSAR phase image and its probability distribution. The dark-bright low-frequency pattern in Fig. 3(a) is the atmospheric effect that ranges from -1.5 to 1.5 rad. Fig. 4(a)–(h) shows the filtered DInSAR phase image using different window sizes of 51×51, 101×101, 151×151, 201×201, 251×251, 301×301, 351×351, and 401×401, respectively. The high-frequency features of ground objects as shown in Fig. 4(a) are reduced as the window sizes increase. Fig. 4(i) shows the changes in the standard deviation of filtered DInSAR phase images as the window size increases, which is the difference in the standard deviations of filtered images using two neighboring window sizes. For example, the value of -0.014 at window size 151 is the difference in the standard deviations between Fig. 4(b) and (c), i.e., the decrease of the standard deviation of the phase image by using the larger filtering window. The changes of standard deviation become steady at approximately -0.09 when the window begins to become larger than 301. The filtered DInSAR phase images in Fig. 4(f)–(h) look similar to one another, indicating that the results with window sizes greater than 301 are consistent. The filtered DInSAR image using window size 301×301 is understood to be atmospheric effects to be removed from the PALSAR InSAR data.

Fig. 5 shows the results of the reduction of atmosphere effects using the proposed method. Fig. 5(a) is the difference between the SRTM-DTM and the PALSAR-DTM that is derived from the corrected InSAR phase. The probability distribution [Fig. 5(b)] shows that the SRTM-DTM is approximately 10 m higher than the PALSAR-DTM. The positions of

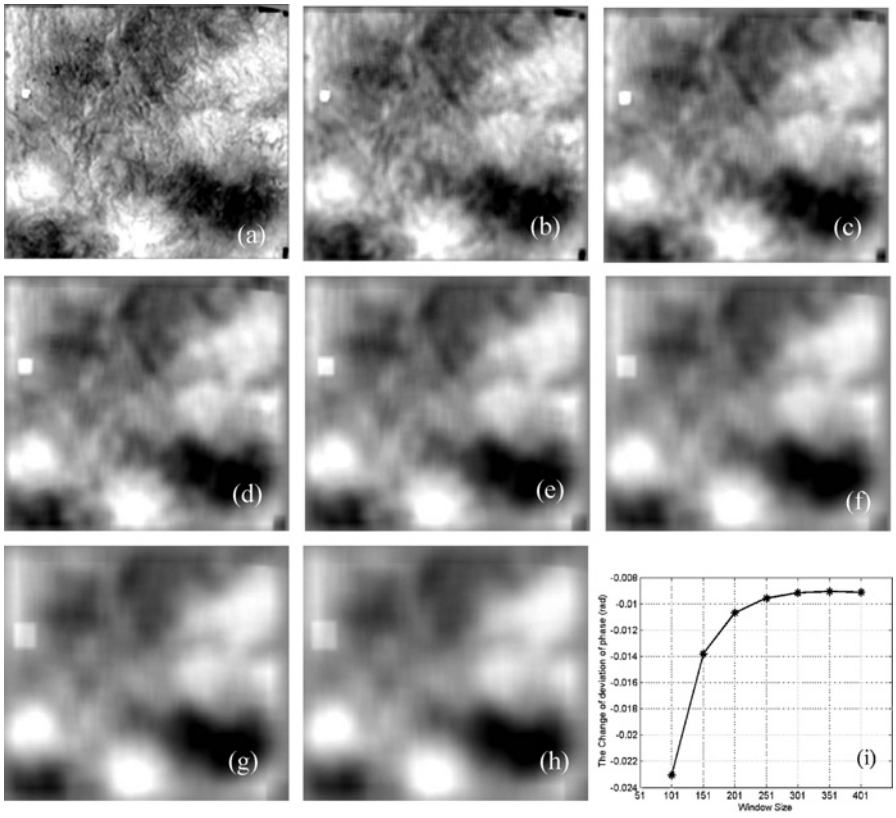

Fig. 4. Results from the low-pass filtering using different window sizes are the following: (a) 51×51; (b) 101×101; (c) 151×151; (d) 201×201; (e) 251×251; (f) 301×301; (g) 351×351; (h) 401×401; (i) Change in the standard deviation and the window size. The standard deviation of (a) is 0.442 while that of (h) is 0.358.

the field sampling plots are shown in Fig. 5(a) as yellow dots. Fig. 5(c) shows enlargements of the area that is delineated by the dashed rectangle in Fig. 5(a); Fig. 5(d) is the subset of the difference image of the SRTM-DTM and the PALSAR-DTM before correction for atmospheric effects. Fig. 5(d) covers the same area with Fig. 5(c). It may be observed that the ground object becomes clear after the atmospheric effects are reduced [Fig. 5(c)]. The 18 polygons shown in Fig. 5(c) and (d) are bare grounds. The mean value of these polygons in Fig. 5(d) is 60.17 m with a standard deviation of 16.26 m; for Fig. 5(c), the mean value of the polygons is 0.52 m with a standard deviation of 4.3 m that indicates the atmospheric effects are substantially reduced. Fig. 5(e) shows the comparison between the measured mean forest height and the height difference of the SRTM-DTM and the PALSAR-DTM in the 18 field sample plots. The stars and circles are the data before and after the corrections for atmospheric effects, respectively. The left and right vertical axes show data after and before correction, respectively. Before the atmospheric correction, the difference between the SRTM-DTM and the PALSAR-DTM does not correlate with mean forest height. After the correction, the correlation of the difference between the SRTM-DTM and the PALSAR-DTM with mean forest height shows values of $R^2 = 0.608$ and RMSE = 4.656 m. Fig. 5(f) is the enlarged image of an area in Fig. 5(a) that is delineated by the solid rectangle, while Fig. 5(g) shows the corresponding mean forest height from the forest inventory map. The polygons of the forest sub-compartments were overlaid in both Fig. 5(f) and (g). The spatial pattern of the difference between the SRTM-DTM and the PALSAR DTM is consistent with the mean forest height from the inventory map.

IV. Discussion

As discussed in Section II above, the determination of the size of the filtering window is important in the proposed method. If the window size is too small, the phase components related to ground objects will remain in the filtered phase image and will be removed from the phase image after correction. Conversely, a portion of the atmospheric effect will remain in the phase image after correction. The changes in the standard deviation of the filtered image as the window size increases are used as the criterion to determine the window size. In this study, the window size increased from 51×51 to 401×401 in 50-pixel intervals. The intervals may be in increments of 10 pixels, 30 pixels or another value, as long as they are constant; if they are not constant, the changes in the standard deviation of the filtered image will become irregular.

As discussed in the Section I, there are currently several methods commonly employed to remove atmospheric effects and assist with measuring terrain deformation using DInSAR data. These methods are based on atmospheric conditions from a GPS signal or from MODIS or MERIS [12]. Although the method proposed in this article may not be as accurate as those based on accurately measured atmospheric conditions, it is a practical method that reduces the primary body of atmospheric effects because it depends only on the SRTM-DTM that is available over terrestrial areas from latitude 56°S to 60°N.

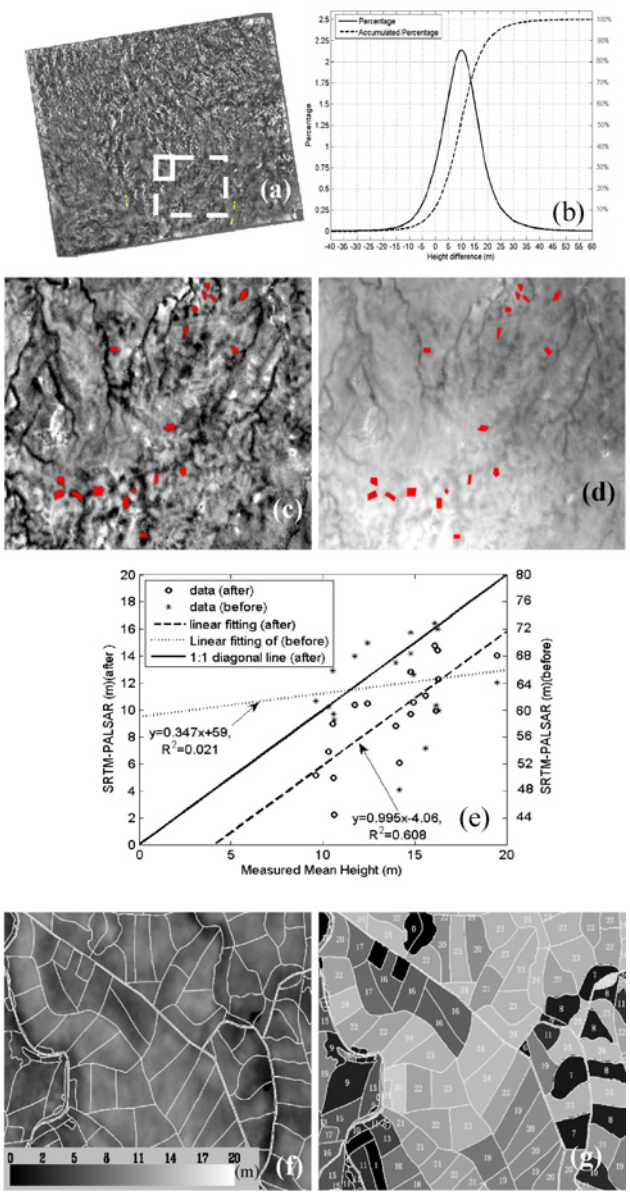

Fig. 5. Results from the application of the proposed method are the following: (a) Geocoded penetration difference map of the SRTM-DTM and the PALSAR-DTM (the points are the 18 field sampling plots) after atmospheric correction; (b) Probability distribution of (a); (c) Subset of the difference map [the area outlined in (a) by the dashed rectangle]; (d) Subset of the difference map before atmospheric correction; (e) Relationship between measured mean forest height and the penetration difference of the SRTM-DTM and the PALSAR-DTM before (dotted line) and after correction (dashed line); (f) Subset of the difference map of the area outlined by the solid rectangle in (a) overlaid by the forest inventory sub-compartment; (g) Mean forest height of sub-compartment from the forest inventory map over the same area as (f).

In fact, the proposed method can use any DEM/DTM that is free of atmospheric effects; the SRTM-DTM is one option. A DEM/DTM from lidar data or photogrammetry, such as ASTER GDEM [13], may substitute for the SRTM-DTM. In addition, the method proposed in this article may also be used to reduce any low spatial frequency feature in the DInSAR phase image caused by factors other than atmosphere.

The improved correlation of the difference between the SRTM-DTM and the PALSAR-DTM with the mean forest height after correction shows that the proposed method may significantly reduce atmospheric effects and make the estimation of mean forest height using penetration difference possible. If the goal is to accurately estimate mean forest height using the penetration difference between SRTM-DTM and PALSAR-DTM data, the influence of the seven-year time span between the acquisition of PALSAR data and SRTM-DTM data should be carefully examined.

V. Conclusion

Atmospheric effects hindered the accuracy and the application of DTMs that are retrieved using spaceborne repeat-pass InSAR data. We proposed a practical method for reducing the atmospheric effect in InSAR data. The method was tested by using the SRTM-DTM and the PALSAR InSAR data. The correlation of the difference between the SRTM-DTM and PALSAR-DTM with mean forest height after removing atmospheric effects showed that the proposed method works well. In our future research, the proposed method will be further examined with other InSAR data, and the influence of forest structure on the HSPC extracted using the proposed method will be investigated.

References

[1] T. Neeff, L. V. Dutra, J. R. dos Santos, C. D. Freitas, and L. S. Araujo, "Tropical forest measurement by interferometric height modeling and P-band radar backscatter," *Forest Sci.*, vol. 51, no. 6, pp. 585–594, 2005.

[2] H. Balzter, C. S. Rowland, and P. Saich, "Forest canopy height and carbon estimation at Monks Wood National Nature Reserve, U.K., using dual-wavelength SAR interferometry," *Remote Sens. Environ.*, vol. 108, no. 3, pp. 224–239, 2007.

[3] J. Kellndorfer, W. Walker, L. Pierce, C. Dobson, J. A. Fites, C. Hunsaker, J. Vona, and M. Clutter, "Vegetation height estimation from shuttle radar topography mission and national elevation datasets," *Remote Sens. Environ.*, vol. 93, no. 3, pp. 339–358, 2004.

[4] H. Balzter, A. Luckman, L. Skinner, C. Rowland, and T. Dawson, "Observations of forest stand top height and mean height from interferometric SAR and LiDAR over a conifer plantation at Thetford Forest, U.K.," *Int. J. Remote Sens.*, vol. 28, no. 6, pp. 1173–1197, 2007.

[5] J. Praks, F. Kugler, K. P. Papathanassiou, I. Hajnsek, and M. Hallikainen, "Height estimation of boreal forest: Interferometric model-based inversion at L- and X-band versus HUTSCAT profiling scatterometer," *IEEE Geosci. Remote Sens. Lett.*, vol. 4, no. 3, pp. 466–470, 2007.

[6] D. Massonnet and K. L. Feigl, "Discrimination of geophysical phenomena in satellite radar interferograms," *Geophys. Res. Lett.*, vol. 22, no. 12, pp. 1537–1540, 1995.

[7] Y. Bock and S. Williams, "Integrated satellite interferometry in southern California," *Eos Trans. Am. Geophys. Union* vol. 78, no. 29, pp. 299–300, 1997.

[8] S. Williams, Y. Bock, and P. Fang, "Integrated satellite interferometry: Tropospheric noise, GPS estimates and implications for interferometric synthetic aperture radar products," *J. Geophys. Res. Solid Earth*, vol. 103, no. B11, pp. 27051–27067, 1998.

[9] A. Ferretti, C. Prati, and F. Rocca, "Nonlinear subsidence rate estimation using permanent scatterers in differential SAR interferometry," *IEEE Trans. Geosci. Remote Sens.*, vol. 38, no. 5, pp. 2202–2212, 2000.

[10] R. Burgmann, P. A. Rosen, and E. J. Fielding, "Synthetic aperture radar interferometry to measure Earth's surface topography and its deformation," *Annu. Rev. Earth Planetary Sci.*, vol. 28, no. 1, pp. 169–209, 2000.

[11] A. Ferretti, C. Prati, and F. Rocca, "Multibaseline InSAR DEM reconstruction: The wavelet approach," *IEEE Trans. Geosci. Remote Sens.*, vol. 37, no. 2, pp. 705–715, 1999.

[12] Z. H. Li, E. J. Fielding, P. Cross, and R. Preusker, "Advanced InSAR atmospheric correction: MERIS/MODIS combination and stacked water vapour models," *Int. J. Remote Sens.*, vol. 30, no. 13, pp. 3343–3363, 2009.

[13] T. Tachikawa, M. Hato, M. Kaku, and A. Iwasaki, "Characteristiacs of ASTERGDEM version 2," presented at the *IEEE Int. Geosci. Remote Sens. Symp. (IGARSS)*, Vancouver, Canada, Jul. 2011.